

RSC Advances



This is an *Accepted Manuscript*, which has been through the Royal Society of Chemistry peer review process and has been accepted for publication.

Accepted Manuscripts are published online shortly after acceptance, before technical editing, formatting and proof reading. Using this free service, authors can make their results available to the community, in citable form, before we publish the edited article. This *Accepted Manuscript* will be replaced by the edited, formatted and paginated article as soon as this is available.

You can find more information about *Accepted Manuscripts* in the [Information for Authors](#).

Please note that technical editing may introduce minor changes to the text and/or graphics, which may alter content. The journal's standard [Terms & Conditions](#) and the [Ethical guidelines](#) still apply. In no event shall the Royal Society of Chemistry be held responsible for any errors or omissions in this *Accepted Manuscript* or any consequences arising from the use of any information it contains.

Imine functionalized thioether Zn(II) turn-on fluorescent sensor and selective sequential logic operations with H_2PO_4^- , DFT computation and live cell imaging

Chiranjit Patra,^a Anup Kumar Bhanja,^a Chandana Sen,^a Durbadal Ojha,^b Debprasad Chattopadhyay,^b Ambikesh Mahapatra,^a and Chittaranjan Sinha^{a*}

Diformyl thioether Schiff base (H_2L) exhibits fluorescence sensor towards Zn^{2+} and the limit of detection (LOD), 0.050 μM , is far below the WHO guideline (76 μM) in drinking water. Formation of 1:1 metal-to-ligand complex, $[\text{ZnL}]$, has been ascertained by X-ray crystallography, Job's plot and Mass spectra. The fluorogenic complex, $[\text{ZnL}]$ (either *in-situ* or solution of isolated complex) has shown selective ON – OFF emission toward H_2PO_4^- . A two-input one-output sequential INHIBIT logic circuit has been constructed from H_2L , Zn^{2+} and H_2PO_4^- . The practical applicability of H_2L has been examined by the identification of Zn^{2+} and H_2PO_4^- in intracellular fluid in living cells (African Monkey Vero Cells).

^aDepartment of Chemistry, Jadavpur University, Kolkata 700 032, India, c_r_sinha@yahoo.com

^bICMR Virus Unit, Infectious Diseases & Beliaghata General Hospital, GB-4, 57, S. C. Bannerjee Road, Beliaghata, Kolkata – 700 010, debprasadc@gmail.com

1. Introduction

Zinc is an essential trace mineral and constitutes more than 250 metalloenzymes.¹ Immune system, sense of taste and smell, DNA synthesis, neural signal transmission, apoptosis regulation, mammalian reproduction, cellular transport, metabolism and overall growth of living body is largely dependent on zinc in biology.² Normal zinc ion concentration in blood plasma of humans is 12–16 μM .³ The imbalance of zinc ion concentration in the cells may lead to pathological processes such as Alzheimer's disease,⁴ epilepsy,⁵ ischemic stroke,⁶ and prostate cancer.⁷ Thus, trace quantity of zinc determination in biology by using chemosensor has received wide attention.⁸ Many Zn^{2+} sensors have been reported in the past⁹ and few of them show “turn-on” fluorescence response. Therefore, it is desirable to develop a chemosensor which could show fluorescence enhancement as well as improved binding selectivity with Zn^{2+} ions in aqueous or mixed aqueous medium. Knowledge of Zn(II) coordination chemistry may help to select donor centres, chelating ligand, flexidenticity, steric and electronic effects. Addition of anions to Zn-sensor complex may influence the emission intensity selectively which may be useful in binary logic operation and can be applied to the signal transduction for the construction of molecular switches.¹⁰ Recently, we have scrutinized vanillyl Schiff base for Zn^{2+} sensor¹¹ and naphthyl appended sulfonamide Schiff base for Al^{3+} sensor.¹² In search of new backbone for the construction of chemosensor 2-hydroxy-5-methylisophthalaldehyde (HMP) has been used.¹³ In this work we have synthesized 3-((Z)-((2-((2-((Z)-(3-formyl-2-hydroxy-5-methylbenzylidene)amino)benzyl)thio)ethyl)thio)phenyl)imino)methyl)-2-hydroxy-5-methyl benzaldehyde (H_2L) by the condensation of 1,2-bis(2-aminophenylthio)ethane and HMP. There are two terminal –CHO groups in a hexadentate $\text{N}_2\text{O}_2\text{S}_2$ type chelation in H_2L which may form two five member M(NS), one five member M(SS) and two six member M(NO) chelate rings upon coordination with a metal ion (M^{n+}) (**Scheme 1**). Presence of chelate rings

of different ring strain could stabilise metal complex because of development of ring polarity. Besides, puckering of a flexidentate chelator is a useful source for the stabilisation of the their steric and polar effects. The composition of Zn^{2+} -sensor complex ($[ZnL]$) has been confirmed by spectroscopic techniques and the isolated complex has structurally been characterized by single crystal X-Ray diffraction measurement. Besides, the product so formed plays INPUT logic operation with $H_2PO_4^-$ at pH 7.2. Among various important anions the presence of phosphate derivatives are considered to be crucial because of their pivotal roles in biological systems¹⁴ and environmental pollution.¹⁵ The measurement of Pi (inorganic phosphate) is an important target for understanding cellular activities involving many active proteins.¹⁶ Pi is used as a food additive in food items such as sausages, crackers, dairy products, and beverages. Besides, a useful fertilizer in agriculture and its high concentration in water cause algal blooming (*eutrophication*) and lowering of dissolved oxygen in water which is fatal to aquatic lives.¹⁷ The high serum concentration of phosphate (> 5.5 mg/dL) can cause adverse renal effects, cardiovascular effects including vascular calcification, and stimulate bone resorption.¹⁸ In addition, Pi can also alter vital cellular signaling process related to cell growth and protein translation. To date, a great number of receptors those are capable of binding and sensing of $H_2PO_4^-$ are known in the literature.¹⁹ The practical applicability of the ligand (H_2L) has been tested in African green monkey kidney cells (Vero cells, ATCC, Manassas, VA, USA) for the determination of exogenous zinc ions by fluorescence cell imaging processes.

2. Experimental Section

2.1. Materials and Methods

All material and reagents were obtained from commercial sources and used without further purification. The sensor, 3-((Z)-((2-((2-((2-((Z)-3-formyl-2-hydroxy-5-

methylbenzylidene)amino)benzyl)thio)ethyl)thio)phenyl)imino)methyl)-2-hydroxy-5-methylbenzaldehyde (H₂L) was synthesised by condensation of 1,2-bis(2-aminophenylthio)ethane with 2-hydroxy-5-methylisophthalaldehyde in methanol medium as per previous procedure.²⁰ Aqueous solutions were prepared using Milli-Q water (Millipore). The complex [ZnL] was synthesised by the reaction of H₂L and Zn(NO₃)₂ · 6H₂O in 1:1 mole ratio in methanol (detail synthesis is given in **(Supplementary Materials, Scheme S1)**). UV-Vis spectra were recorded on Perkin Elmer Lambda 25 spectrophotometer and fluorescence spectra were obtained from Perkin Elmer Spectrofluorimeter model LS55; FT-IR spectra (KBr disk, 4000–400 cm⁻¹) from a Perkin Elmer LX-1FTIR spectrophotometer. NMR spectra were obtained on a Bruker (AC) 300 MHz FT-NMR spectrometer using TMS as an internal standard. ESI mass spectra were recorded from a Water HRMS model- XEVO-G2QTOF#YCA351 Spectrometer. All of the measurements were conducted at room temperature.

2.2. X-Ray Crystallography of [ZnL]

Single crystals of [ZnL] suitable for data collection were grown from slow evaporation of DMF-CH₃CN (v/v, 1:1) solution. The crystal data and details of the data collections are given in **(Supplementary Materials, Table S1)**. Suitable single crystal of the complex (0.16 x 0.09 x 0.06 mm) was mounted on a Bruker SMART APEX CCD diffractometer (graphite monochromated MoK α radiation, $\lambda = 0.71073 \text{ \AA}$) and data were collected by use of ω scans. Unit cell parameters were determined from least-squares refinement of setting angles (θ) within the range $1.72 \leq \theta \leq 28.01$. Data were corrected for Lorentz polarization effects and for linear decay. Semi-empirical absorption corrections based on ψ -scans were applied. The structures were solved by direct method using SHELXS-97 and successive difference Fourier synthesis within hkl range $-33 \leq h \leq 33$, $-9 \leq k \leq 9$, -21

$\leq 1 \leq 21$. All non-hydrogen atoms were refined anisotropically. The hydrogen atoms were fixed geometrically and refined using the riding model. All calculation was carried out using SHELXL-97,²¹ ORTEP-32²² and PLATON-99²³ programs.

2.3. Theoretical computation

H₂L and [ZnL] were optimized to generate the structures by DFT/B3LYP method using Gaussian 09 software.²⁴⁻²⁶ 6-311G+(d, p) basis set were used for C, H, N, O and Lan12dz basis set was used as effective potential (ECP) set for Zn and S.²⁷⁻²⁹ To ensure the optimized geometries represent the local minima the vibrational frequency calculations were performed and these were only positive eigen values. Theoretical UV-Vis spectra were calculated by time-dependent-DFT/B3LYP method in methanol using conductor-like polarizable continuum model (CPCM).³⁰⁻³² GAUSSSUM was used to calculate the fractional contributions of various groups to each molecular orbital.³³ DFT/B3LYP-excited model was used for triplet state analyses of the molecules.³⁴

2.4. Immunofluorescence (IFA) Examination

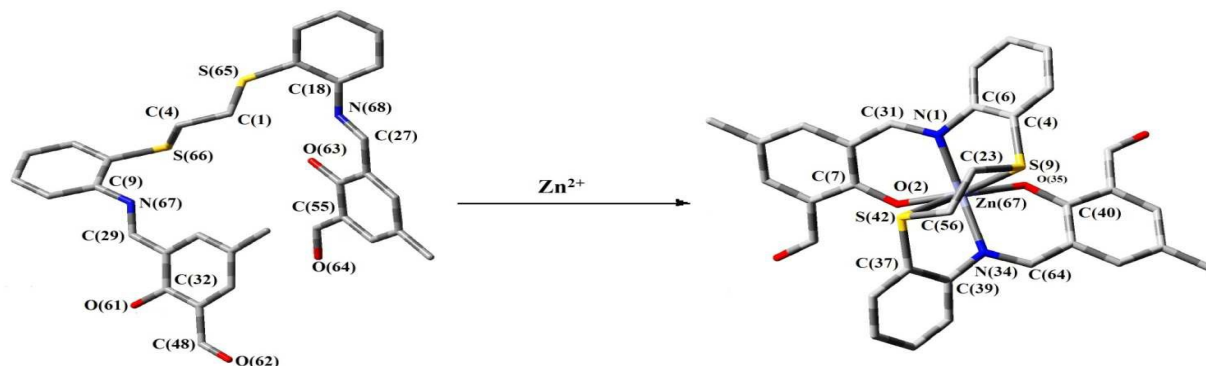
The Eagle's minimum essential medium (EMEM) was used to prepare African green monkey kidney cells (Vero cells, ATCC, Manassas, VA, USA) in 5–10% feta bovine serum (FBS). Vero cells monolayer (1.0×10^6 cells/ml) was grown onto 6 well plates at 5% CO₂ for 24 h. The cells were fixed in paraformaldehyde (4%) solution and blocked with 1% bovine serum albumin (BSA) in 0.1% PBS (phosphate buffered saline)-triton-X100 solution. These were washed and permeabilized with 0.1% Triton-X100 in PBS. H₂L (100 µg/ml) was treated with permeabilized Vero cells monolayer for 1h at room temperature and was washed twice with PBS (pH 7.2) to eliminate cell rubbish. After washing with PBS, Zn²⁺ (Zn(NO₃)₂ · 6H₂O, 100 µg/ml) was added in drops via micro-syringe for 10 min, and washed twice with PBS. Under similar condition NaH₂PO₄ (100 µg/ml) in aqueous medium was added in presence of

Zn(NO₃)₂ and H₂L to permeabilized Vero cells monolayer for 1h at room temperature. Then, the cells were observed under epifluorescence microscope.³⁵

3. Results and discussion

3.1. The characterisation of sensor, H₂L and its complex, [ZnL]

The condensation of 2-hydroxy-5-methylisophthalaldehyde with 1,2-bis(2-aminophenylthio)ethane has synthesised 3-((Z)-((2-((2-((Z)-((Z)-3-formyl-2-hydroxy-5-methylbenzylidene)amino)benzyl)thio)ethyl)thio)phenyl)imino)methyl)-2-hydroxy-5-methyl benzldehyde (H₂L) (**Supplementary Material, Scheme S1**).²⁰ It has been characterised by spectroscopic data (NMR, Mass, FTIR; (**Supplementary Material, Figs, S1-S3**). Molecular ion peak, (H₂L+H)⁺ 569.20 supports the molecular identity which has been supported by $\nu(\text{C}=\text{N})$ at 1618 cm⁻¹ and $\nu(\text{CHO})$ at 1677 cm⁻¹ of IR spectrum. The ¹H NMR spectrum of H₂L (300 MHz, DMSO-d₆) demonstrates singlet at 14.05 ppm corresponds to $\delta(\text{OH})$; imine-H (CH=N) appears at δ 8.98 ppm; $\delta(\text{CHO})$ is observed at 10.42 ppm and aromatic protons appear at 7.18-7.77 ppm. The reaction of H₂L with Zn(NO₃)₂ · 6H₂O in methanol has isolated mononuclear zinc complex, [ZnL] (**Supplementary Material, Scheme S1**). The complex, [ZnL], has shown $\nu(\text{C}=\text{N})$ at 1589 cm⁻¹ which is shifted to lower energy compared to H₂L and $\nu(\text{CHO})$ at 1648 cm⁻¹ and also molecular ion peak of Mass spectrum (630.17) (Mass, FTIR; **Supplementary Material, Figs. S4, S5**) and support the composition of the complex. The structure has been confirmed by single crystal X-ray crystallography.



**Scheme 1** DFT optimized structures of H₂L and its Zn(II) complex

The molecular structure of [ZnL] is shown in **Fig. 1** with the atom numbering pattern and the selected bond distances and angles are measured. The crystal is monoclinic system and the space group is C2/c. In the complex Zn(II) is sitting at the distorted octahedron centre with Zn(ONS)₂ arrangement. A basal plane is considered with N₂OS while two axial positions are occupied by remaining O and S donor centres. Zn(1) is deviated by ~ 0.2 Å from the square plane constituted by N₂OS towards O(phenolato) axial side. The imine length, C(8)=N(1), is 1.287(3) Å which is comparable to literature report.³⁶⁻³⁹ The bond lengths in the coordination zone are Zn(1)-N(1), 2.089(2); Zn(1)-O(1), 1.9628(16); Zn(1)-S(1), 2.6800 (7) Å. The Zn-S distance is closer to the literature data (2.6100(13) Å)³⁷ but shorter than those of sum of the van der Waals radii of Zn (1.39 Å) and S (1.80 Å) which implies bonding interaction. The important angles are ∠N(1)-Zn(1)-O(1), 98.09(7)°, 90.00(7)° (symmetry : -x,y,1/2-z); ∠S(1)-Zn(1)-S(1), 81.80(3)°; ∠N(1)-Zn(1)-S(1), 77.70(5)°, 92.08(5)° (symmetry : -x,y,1/2-z); ∠S(1)-Zn(1)-O(1), 87.29(5)°, 163.18(5)° (symmetry : -x, y, 1/2-z) and ∠N(2)-Zn(1)-N(1), 166.57(10)°. Two intermolecular recognisable hydrogen bonds are observed at C(41E) – H(41A)---O(2) (H41E---O(111), 2.5600 Å; C(41E)---O(2), 3.440(5) and ∠C(41E) – H(41A)---O(2), 152.00°; symmetry : 1/2-x, 1/2-y, 1-z) and C(47E)–H(47A)---O(1) (H(47E)---O(1), 2.3500 Å; C(47E)---O(1), 3.251(3) Å and ∠C(47E) – H(47A)---O(1), 155.00°; symmetry : -x, 1+y, 1/2-z) who are useful to generate 1D chain in solid phase (**Fig. 2**).

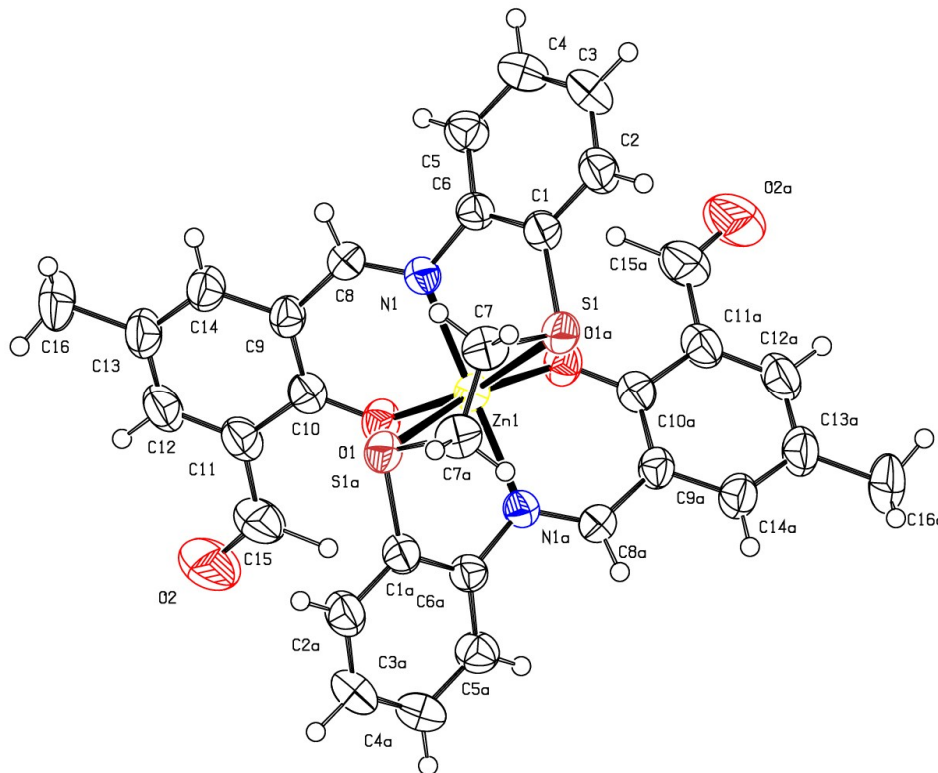


Fig.1 Molecular structure of the complex, [ZnL]. Bond distances in coordination sphere : Zn(1)-N(1), 2.089(2); Zn(1)-O(1), 1.9628(16); Zn(1)-S(1), 2.6800 (7), C(8)-N(1), 1.287(3) Å; bond angles (symmetry) : \angle N(1)-Zn(1)-O(1), 98.09(7) $^\circ$, 90.00(7) $^\circ$ (-x,y,1/2-z); \angle S(1)-Zn(1)-S(1), 81.80(3) $^\circ$; \angle N(1)-Zn(1)-S(1), 77.70(5) $^\circ$, 92.08(5) $^\circ$ (-x,y,1/2-z); \angle S(1)-Zn(1)-O(1), 87.29(5) $^\circ$, 163.18(5) $^\circ$ (-x,y,1/2-z) and \angle N(2)-Zn(1)-N(1), 166.57(10) $^\circ$.

The DFT optimized structure of [ZnL] (**Scheme 1**) has been generated and the structural identity has been compared with single crystal X-ray determined structure. Bond parameters calculated from optimised structure (DFT computation) is closer to the experimental results; the bond lengths vary within 0.01 – 0.04 Å and bond angles vary 4-8 $^\circ$. Weak bonds are conveniently response to physical, optical, chemical signals and may be useful in the identification of selective and specific ions or molecules.

Theoretical structure of H₂L has also similarly generated and the characteristics have been verified by calculating vibrational frequencies of some of the functions and on

comparing with experimental spectra. The calculated metric parameters such as bond lengths of C=N (1.281 Å (H₂L); 1.327 Å (ZnL) Å), C-O (1.36 Å (H₂L); 1.42 Å ([ZnL]), Zn-N (2.130 Å), Zn-O(phenolic) (1.977 Å), Zn-S(thioether) (2.975 Å) etc. and angles (∠N-Zn-O, 90.63°; ∠S-Zn-S, 74.95°, ∠O-Zn-O, 120.59°, ∠N-Zn-N, 156.85° etc. (**Supplementary Materials, Tables S2 and S3**) are comparable with similar structures in literature.³⁶⁻³⁹ The binding of Zn²⁺ enhances the bond lengths of C=N and C-O which may be due to the electron drifting of metal ion from L²⁻. This is also supported by lowering of $\nu(\text{C}=\text{N})$ in [ZnL] compared to H₂L.

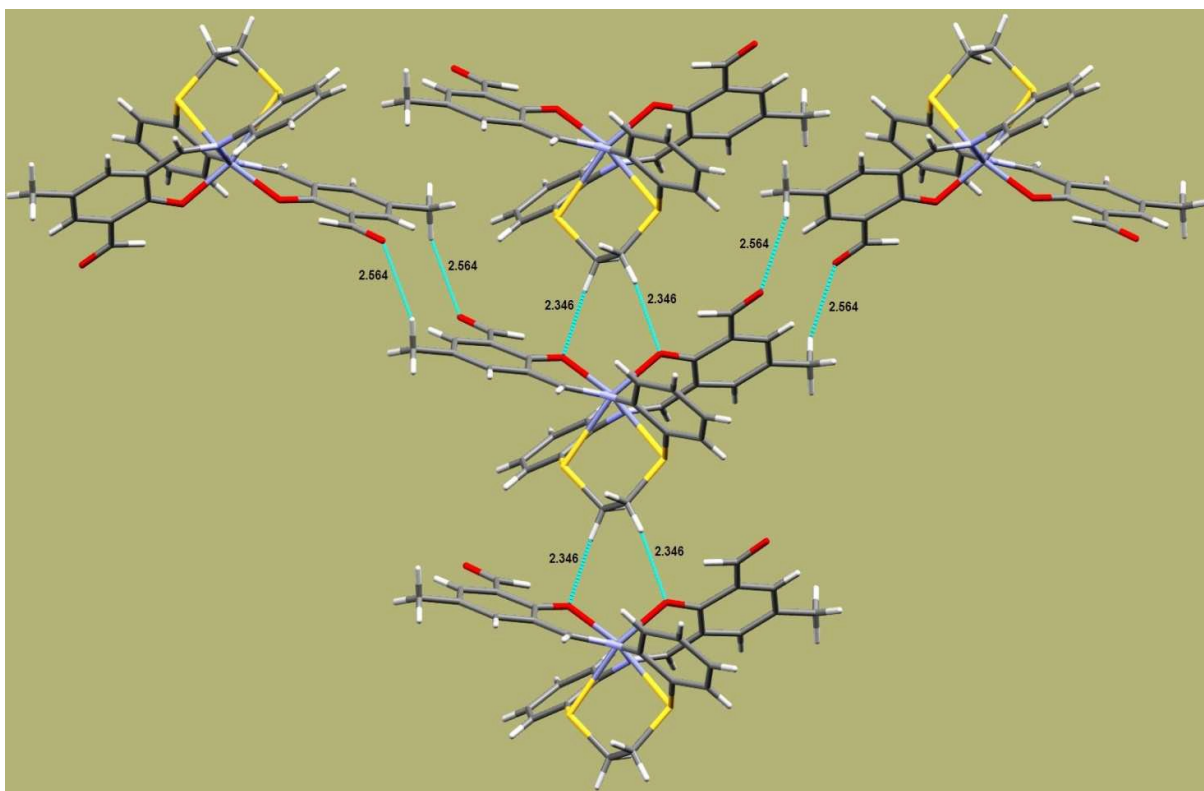


Fig. 2 Hydrogen bonded 1D supramolecular chain of ZnL

3.2. Zn²⁺ sensor activity : UV-Vis Spectroscopic studies

The UV-vis spectrum of H₂L in aqueous-MeOH (v/v, 1/2) buffer solution (0.01 M, pH 7.2, HEPES; v/v = 1/2) has exhibited two sharp bands at 289 and 375 nm. These bands may be assigned to the intraligand charge transfer transitions. The titration of H₂L with incremental addition of Zn²⁺ has been recorded in HEPES buffer (10 mM, pH - 7.2) at 25°C in the same solvent which has shown absorption enhancement at 447 nm and decrement at 375 nm with isobestic at 408 and 332 nm (**Fig. 3**). Naked eye colour change of H₂L solution upon addition of Zn²⁺ ion is very amazing (**Supplementary Material, Fig. S6**). The red shifting of the bands of H₂L upon Zn²⁺ addition is attributed to an intramolecular charge transfer (ICT) through the chelation to Zn²⁺ (**Fig. 1**).

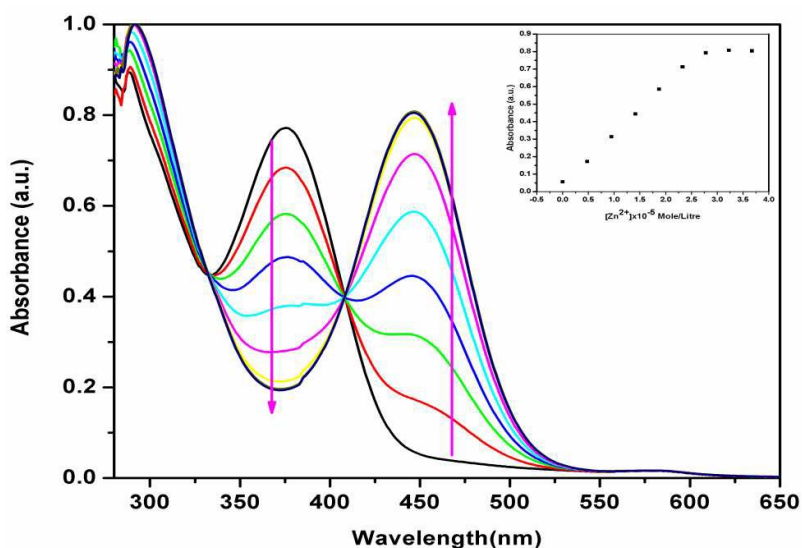


Fig.3 Change in absorption spectra of H₂L (50 μM) upon addition of Zn²⁺ in MeOH/water (v/v, 2:1); non-linear plot of absorbance (at 447 nm) vs. [Zn²⁺] for the corresponding UV-Visible titration is shown inset

The incremental addition of Zn²⁺ shows increase in absorbance till the ratio of [Zn²⁺] : [H₂L] reaches 1 : 1, and no longer changes with continuous addition of excess of Zn²⁺. The composition has been checked by Job's plot from the solution mixture (**Supplementary**

Material, Fig. S7). The association constant of H₂L with Zn²⁺ is $13.47 \times 10^4 \text{ M}^{-1}\text{L}$. Due to complexity of the intracellular environment, further examination has been conducted to account on the interferences of other ions. Selective metal ion assays were performed while keeping the other experimental condition unchanged.

The spectroscopic study has been performed to control the efficiency of the probe (H₂L) at optimum pH. Fluorescence emission of H₂L is indifferent in the experimental pH range of 2-12 (**Supplementary Material, Fig. S8**). However, the presence of Zn²⁺ to the solution of H₂L enhances the emission intensity and has reached highest emission at pH 8.0; further increase in pH reduces the emissivity which may be due to breakdown of geometry of the complex structure.

3.3. Fluorescence OFF-ON sensing for Zn²⁺

The probe (H₂L) exhibits weak emission at 575 nm (**Supplementary Material, Fig. S9**) which may be due to PET (photoelectron transfer) from the phenolic –OH to imine-N and/or -CHO when excited at 375 nm in HEPES buffer (10 mM, pH - 7.2;) at 25 °C in MeOH-water (v/v, 2:1). Upon addition of Zn²⁺ to the solution of probe (H₂L) enhances the emission intensity at 530 nm. Fluorescence augmentation on addition of Zn²⁺ to the probe may be due to exclusion of PET and/or ICT and also by chelation effect which improves molecular rigidity and is defined as chelation enhancement of fluorescence (CHEF, **Supplementary Material, Scheme S2**). The complexation of H₂L with Zn²⁺ has been supported by isolation and structural characterisation of the complex, [ZnL] (**Fig. 1**). Moreover, no significant change in emission spectra is observed even after addition of excess (5 equivalents) metal ions: Na⁺, K⁺, Ca²⁺, Mg²⁺, Mn²⁺, Fe³⁺, Al³⁺, Co²⁺, Ni²⁺, Pd²⁺, Cd²⁺, Hg²⁺, Cu²⁺, Ba²⁺ and Pb²⁺ (**Fig. 4**). In the fluorescence titration, the result shows that none of these metal ions significantly affect the emission intensity of the Zn²⁺ complex. Therefore,

the probe recognises Zn^{2+} selectively in the presence of other metal ions (**Supplementary Material, Fig. S10**) and also intensity enhances with increasing concentration of Zn^{2+} (**Fig. 5**). The quantum yield of probe ($\Phi_{\text{H}_2\text{L}}$, 0.0012) is much lower than that the complex, $[\text{ZnL}]$ (Φ_{ZnL} , 0.052). The binding constant (K_d , $13.47 \times 10^4 \text{ M}^{-1}\text{L}$) has been determined by fitting fluorescence data as a function of metal ion concentration to a suitable computer-fit nonlinear program (**Supplementary Material, Fig. S11**). The limit of detection (LOD) of Zn^{2+} has been determined by $3\sigma/m$ method and found to be as low as $0.050 \mu\text{M}$ (**Supplementary Material, Fig. S12**). There are enormous numbers of reports on Zn^{2+} -sensors with basic

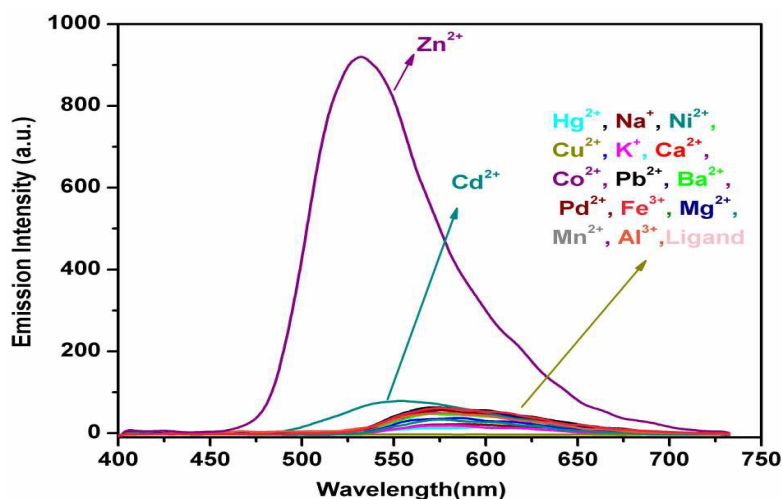


Fig.4 Fluorescence ($\lambda_{\text{ex}} = 375 \text{ nm}$) responses of H_2L upon addition of various metal ions in HEPES buffer (10 mM, pH - 7.2;) at $25 \text{ }^\circ\text{C}$ in MeOH/water (v/v, 2:1) at emission slit 8 nm.

fluorogenic motive like quinoline (LOD, $0.12 \mu\text{M}$),^{40, 41} imidazo[1,2-a]pyridine (LOD, $0.068 \mu\text{M}$)⁴² pyridyl system (LOD, 17 – $400 \mu\text{M}$),⁴³ bipyridyl (LOD, $0.78 \mu\text{M}$),^{44,45} naphthyl (LOD, $0.13 \mu\text{M}$),⁴⁶ pyrenyl derivatives (LOD, $0.08 \mu\text{M}$),⁴⁷ terphenyl-based motif (LOD, $0.10 \mu\text{M}$),⁴⁸ pyrimidinyl based Schiff-base (LOD, $0.69 \mu\text{M}$),⁴⁹ pyrazoline (LOD, 0.20

- 0.61 μM),^{50,51} BINOL (LOD, 2.2 μM),⁵² rhodamine (LOD, 0.5-0.15 μM),^{53,54} and - vanillinyl thioether Schiff base (LOD, 0.018 μM).¹⁶ Since, the probe in this report, H₂L, contains N, O, S donor centres and of them exocyclic imine-N and S are soft and according to HSAB principle, soft donor centres prefer soft metal centre for strong binding. This may be one of the reasons to play an important role in the recognition of Zn²⁺ in presence of large number of cations. All these facts indicate that H₂L serves as an efficient fluorogenic chemosensor for Zn²⁺ recognition.

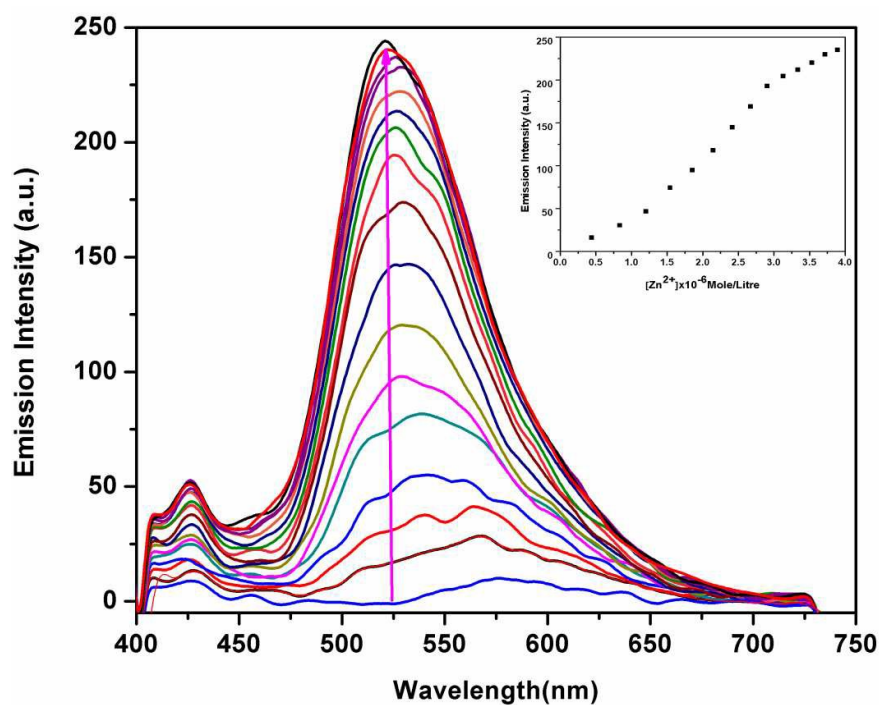


Fig. 5 A. Change in fluorescence intensity of H₂L upon addition of 50 μM Zn²⁺ at emission slit 5 nm; non-linear plot of fluorescence intensity (at 530 nm) vs [Zn²⁺] for the corresponding fluorescence titration (*inset*).

The molecular functions obtained from DFT computed optimized structures of H₂L and [ZnL] has been used to explain red shifting of charge transfer transitions in the absorption spectra upon complexation. The molecular functions (both occupied and unoccupied) are

mainly composed of ligand orbitals (>90%) (Supplementary Materials, Tables S4, S5). The energy difference between HOMO and LUMO is decreased from 3.51 eV in H₂L to 3.34 eV in the complex, [ZnL] (Fig. 6) this may support the shifting of absorption band to longer wavelength on coordination to Zn²⁺ (375 nm in H₂L shifts to 447 nm in [ZnL]). Thus HOMO → LUMO in H₂L and HOMO-1 → LUMO (f, 0.5037) and HOMO-6 → LUMO (f, 0.1631) in the complex, [ZnL] are intraligand charge transferences.

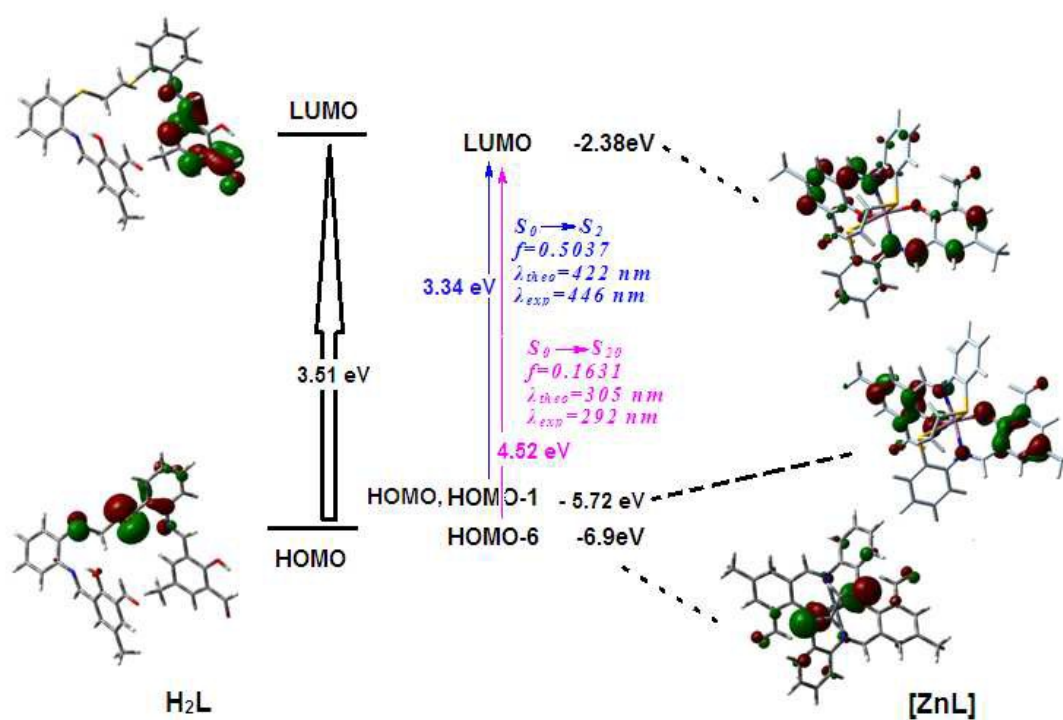


Fig.6 Correlation between HOMO and LUMO functions of H₂L and [ZnL].

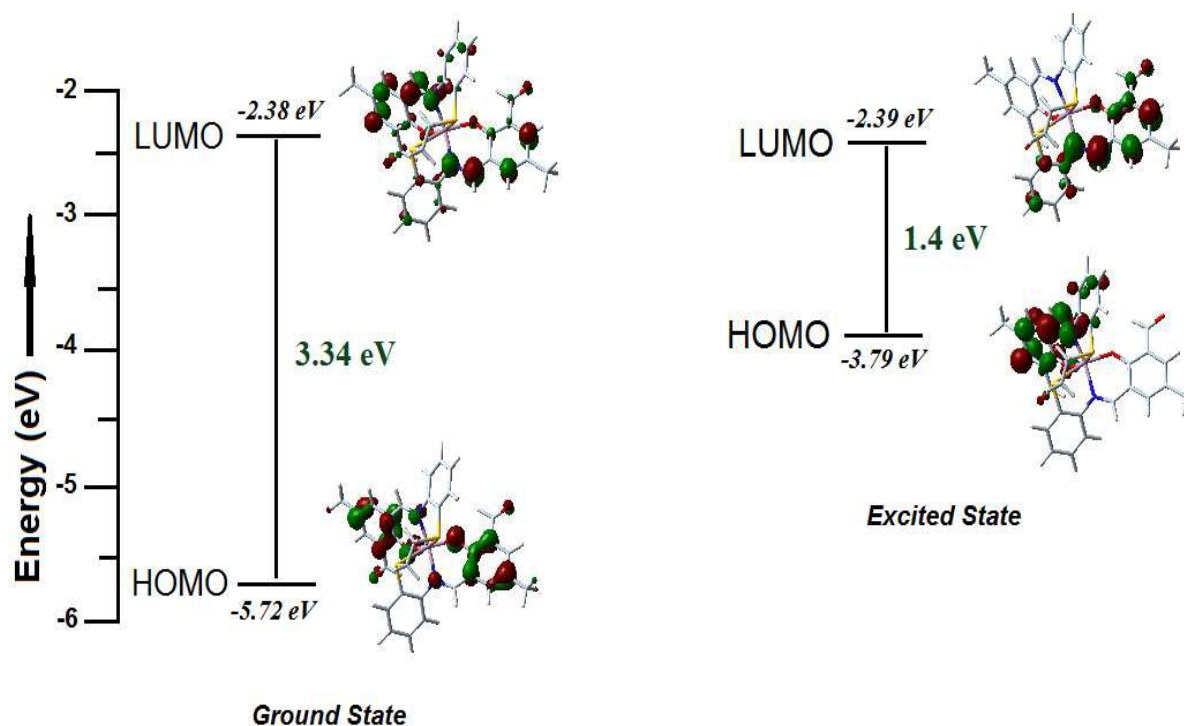


Fig. 7 Excited state functions of optimized geometry at T_1 phase and their transition probabilities

The T_1 state of [ZnL] is optimized and it is observed that the HOMO in T_1 phase is destabilized by 1.93 eV compared to that in S_0 state (**Supplementary Materials. Table S6, S7**). As a result, the energy difference between the HOMO and LUMO is decreased by 1.4 eV while it is 3.34 eV in S_0 state. The geometry relaxation may be the main origin of the large Stoke shift (**Fig. 7**). The calculated emission energies, dominant configurations (with larger CI coefficients), transition nature, and the available experimental values are listed in **Table 1**. For [ZnL] the calculated fluorescence wavelength is 492.88 nm, which is close to the experimental value 530 nm .

Table 1 Ground state and triplet excited state of [ZnL] in MeOH using DFT and TD-DFT computation of CPCM model

Process	Electronic transitions	Composition	Excitation energy (eV)	Oscillator strength, $f(\lambda_{cal})$	CI	λ_{exp} (nm)
Absorption	$S_0 \rightarrow S_{20}$	HOMO-6 \rightarrow LUMO	4.0585	0.1631 (305.49)	0.55641	292
	$S_0 \rightarrow S_2$	HOMO-1 \rightarrow LUMO	2.9405	0.5037 (421.65)	0.55246	447
Emission	$S_1 \rightarrow S_0$	HOMO \rightarrow LUMO+5	2.6143	0.3486 (492.88)	0.87357	530

3.4. Performance of [ZnL] for the sensing of $H_2PO_4^-$

To examine the anion recognition of [ZnL], different anions such as : PO_4^{3-} , AMP, ATP, $P_2O_7^{4-}$, $H_2PO_4^-$, $C_6H_5O_7^{3-}$, AsO_4^{3-} , AsO_3^{3-} , AsO_2^- , CH_3COO^- , F^- , Cl^- , Br^- , I^- , SCN^- , $S_2O_3^{2-}$, ClO_4^- , SO_4^{2-} , NO_2^- , N_3^- etc are added individually to the solution of the complex (**Fig. 8**). Among the aforesaid anions, only $H_2PO_4^-$ has induced a conspicuous change in the absorptive and emissive behaviour of the complex. Interestingly, the yellow color of [ZnL] turned colorless with the addition of $H_2PO_4^-$ ions only (**Fig. 9**). The UV-Vis absorption response of [ZnL] towards $H_2PO_4^-$ is shown in **Fig. 10** and it is observed that the band at 447 nm characteristics to the complex, [ZnL], is decreased, while the band at 375 nm is recovered gradually upon addition of $H_2PO_4^-$ which is the characteristic to free ligand, H_2L . In the fluorescence spectrum, the band intensity at 530 nm corresponds to [ZnL] is decreased upon addition of $H_2PO_4^-$ (**Fig. 11**). Fluorescence titrimetric measurement shows that 2 equivalent of $H_2PO_4^-$ per [ZnL] (**Fig. 11**) has been required for completion of the reaction which could suggest the formation of $[Zn(H_2PO_4)_2]$. This spectral observation may infer that $H_2PO_4^-$

insists selective dechelation of the sensor from [ZnL]. It is interesting to note that PO_4^{3-} , HPO_4^{2-} , AMP, ATP, $\text{P}_2\text{O}_7^{4-}$ do not affect the emission characteristics of [ZnL] (**Fig. 8**). H_2PO_4^- may assist hydrogen bonding interaction with pendant $-\text{CHO}$ group of the sensor and may come closer to the Zn^{2+} in the complex, [ZnL], which may help exclusion of metal ion, and hence the recovery of free ligand emission characteristics is observed.^{55,56} Subsequent, ESI-MS measurement of the mixture ([ZnL] + KH_2PO_4) shows the presence of strong mass peak corresponds to KH_2L^+ (m/z, 607) and may support above proposal (**Supplementary Material; Fig. S13**).

Lifetime data are obtained upon excitation at 370 nm and the fluorescence decay curve was deconvoluted with respect to the lamp profile. The observed fluorescence decay fits nicely with bi-exponential decay profile for the complexes (**Fig. 12**) which is supported by goodness-of-fit (χ^2) data in the regression analyses. Radiative and non-radiative rate

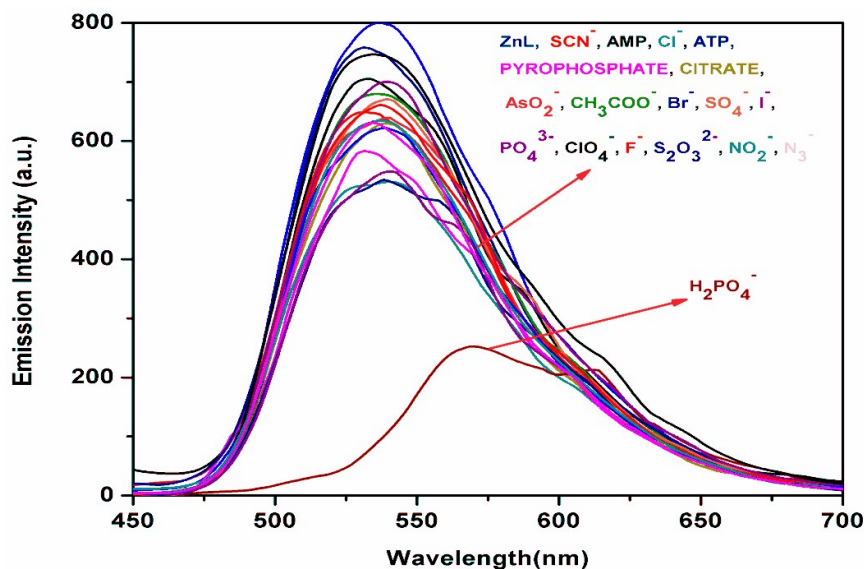


Fig. 8 Fluorescence emission spectra of the of [ZnL] upon addition of different anions (5 equivalent of PO_4^{3-} , AMP, ATP, $\text{P}_2\text{O}_7^{4-}$, H_2PO_4^- , $\text{C}_6\text{H}_5\text{O}_7^{3-}$, AsO_4^{3-} , AsO_3^{3-} , AsO_2^- , CH_3COO^- , F^- , Cl^- , Br^- , I^- , SCN^- , $\text{S}_2\text{O}_3^{2-}$, ClO_4^- , SO_4^{2-} , NO_2^- , N_3^-)



(a)



(b)

Fig. 9. (a) Naked eye absorption change and (b) fluorescence change of [ZnL] (50 μ M in aqueous-MeOH (v/v, 1/2) upon the addition of 2 eq. of various anions (1.5 mM in H₂O).

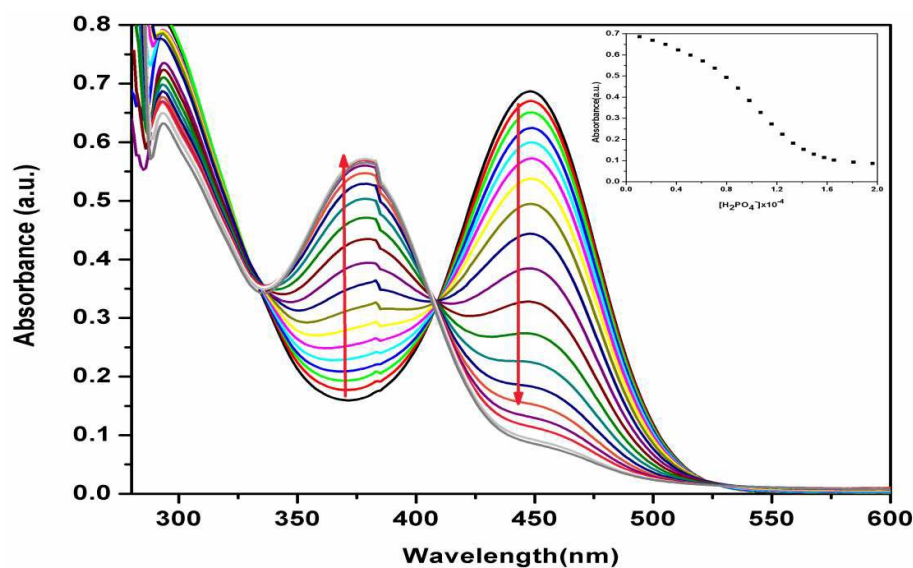


Fig. 10 (A) Change in absorption spectra of H₂L-Zn²⁺ system upon addition of H₂PO₄⁻ in MeOH/water (v/v, 2:1); (B) Non linear plot of absorbance (at 447 nm) vs. [H₂PO₄⁻] for the corresponding UV-Visible titration

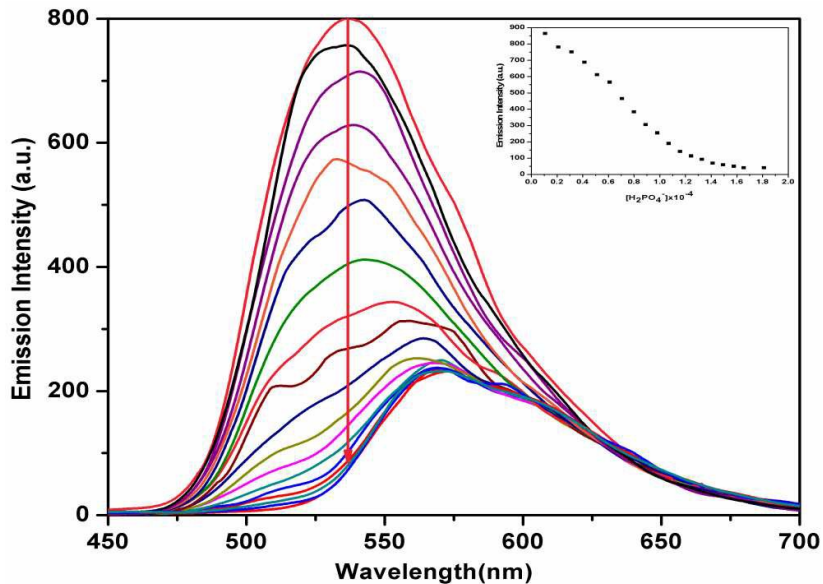


Fig. 11 Fluorescence titration spectra of the [ZnL] complex with gradual addition of H_2PO_4^- ; non-linear plot of fluorescence intensity (at 530 nm) vs. $[\text{Zn}^{2+}]$ for the corresponding fluorescence titration (*inset*).

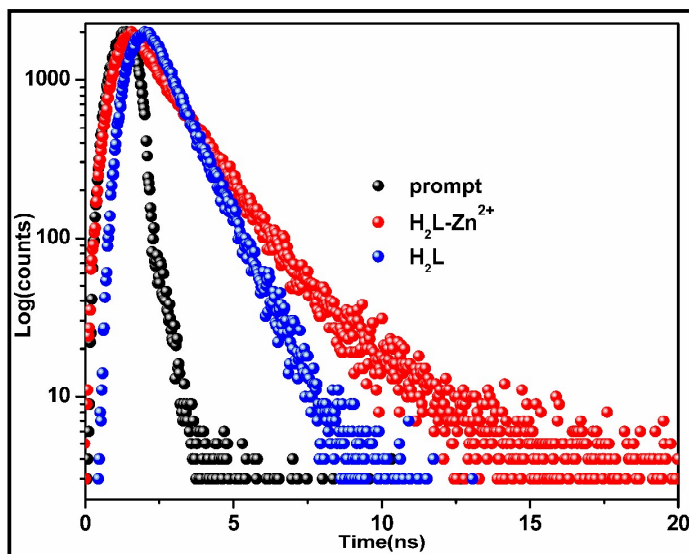


Fig. 12 Fluorescence life time decay of H_2L and the [ZnL] complex

constants (k_r and k_{nr} ; **Supplementary Material, Table S8**) are calculated and data show usual higher k_{nr} than k_r value. The average lifetime value of [ZnL] (0.255 ns) is longer than H₂L (0.162 ns) data. The metal-ligand orbital mixing in [ZnL] may be the reason for passing longer time at excited state.

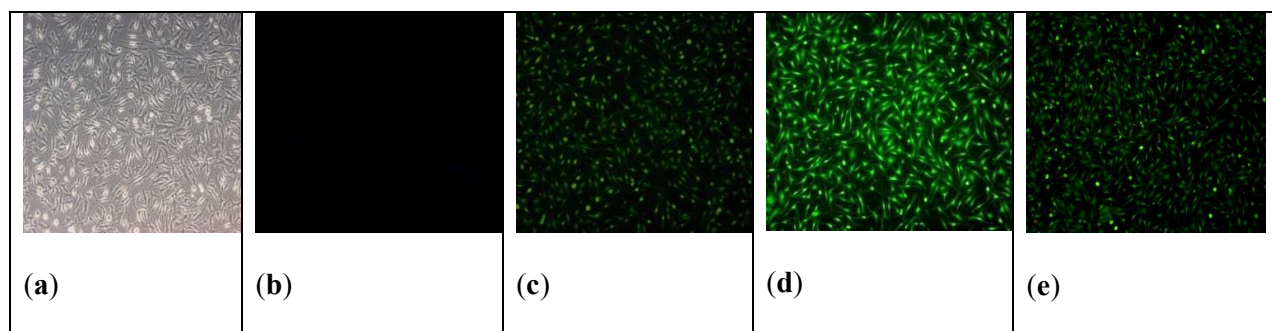
3.5. Application as logic function

Following the principle of binary logic operation, the truth table is constructed using the three basic logic operations (AND, NOT, and OR) and more complex logic functions (EOR, INH, NOR, XNOR, and XOR) have been reproduced at the molecular level. Light sensitive single molecules are very useful to assemble integrated logic gates such as INHIBIT, half-subtractor, half-adder, full-adder, and full-subtractor.⁵⁷ INHIBIT logic deserves some attention because it demonstrates a noncommutative behaviour.⁵⁸ This means that one input has the power to disable the whole system, that is, it holds a veto. The fluorescence properties of H₂L can be applied to construct INHIBIT logic gate. With two inputs as Zn²⁺ and H₂PO₄⁻, H₂L has the ability to exhibit INHIBIT function *via* both absorption as well as emission output (**Scheme 2**). When Zn²⁺ is present in the solution the absorption as well as emission at 447 nm and 530 nm respectively is 1 while the values of all other functions are 0. Thus the absorption change at 447 nm and emission change at 530 nm with Zn²⁺ as well as H₂PO₄⁻ as inputs can be described as a monomolecular circuit showing an INHIBIT

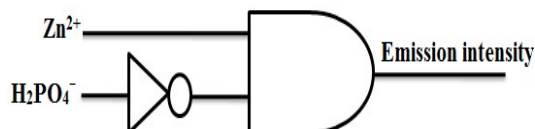
3.6. Cell Imaging Studies

Vero cells (African green monkey kidney cells) are used to explore the effect of probe, H₂L towards the recognition of ions in biological systems. The fluorescence imaging of intracellular Zn²⁺ in living cells is shown in **Fig.13**. Vero cells fixed in paraformaldehyde

(4%) and blocked with BSA in PBS-triton X100 solution. Then, the cells were observed under epifluorescence microscope. Then, the cells were treated with Zn^{2+} solution (30 mM) for 45 min in buffer for incubation, washed again with buffer at pH (7.2) and mounted on a grease free glass slide. Cells were observed under a fluorescence microscope equipped with a UV filter after adding H_2L (2 mM). Cells incubated only with Zn^{2+} were used as a control.



H_2PO_4^-	Zn^{2+}	OUTPUT (Emission Intensity)
0	0	0 (Low)
1	0	0 (Low)
0	1	1 (High)
1	1	0 (Low)



Scheme 2 Logic gate and truth table.

Fig. 13 Fluorescence microscopic images of Vero cells: (a) Untreated Cell control; (b) Cell under fluorescence microscope; (c) Cells treated with H_2L in bright field; (d) Cell treated with Zn^{2+} (10 μM for 1 h at 37°C) and exposed to H_2L for 10 min; (e) Cell treated with Zn^{2+} (10 μM for 1 h at 37°C) and NaH_2PO_4 (20 μM) and exposed to H_2L for 10 min.

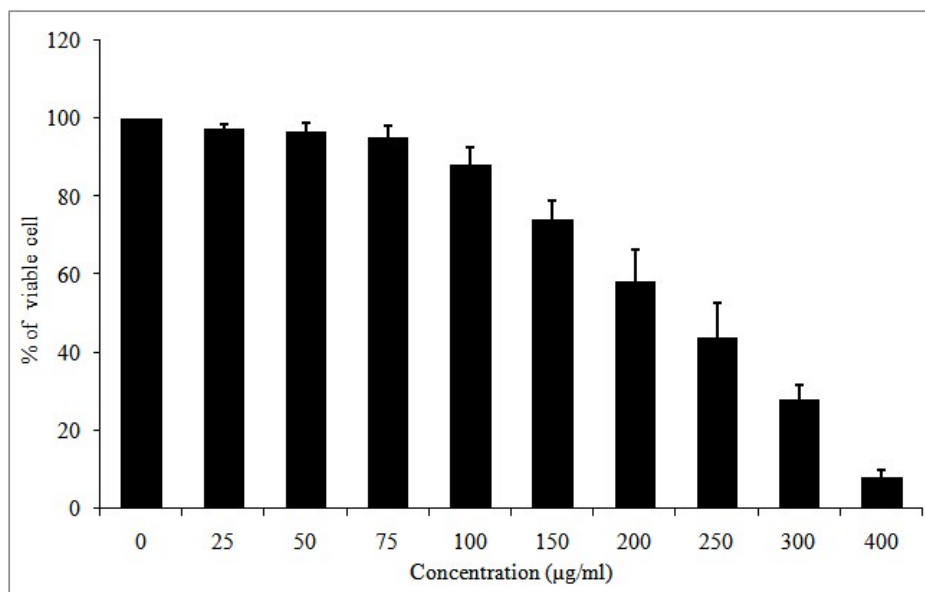


Fig. 14 Cell viability data (MTT assay) of H₂L

H₂L can permeate easily through tested living cells without any harm (as the cells remain alive even after 30 min of exposure to H₂L at 2 mM). The MTT assay has been applied for labelling dead cells to evaluate cytotoxicity of the probe (**Fig. 14**). The study shows that H₂L has no cytotoxicity towards cells upto 75 µg/ml (approx). These results indicate that the probe has a huge potential in both *in vitro* and *in vivo* applications as a Zn²⁺ sensor and in live cell imaging.

4. Conclusion

Thioether Schiff base with appended –CHO group (H₂L), a N₂O₂S₂ hexadentate probe exhibits red-shifting of absorption band 375 nm to 447 nm upon Zn²⁺ addition. Fluorescence emission has been enhanced by 240 times in presence of Zn²⁺ at 530 nm and the limit of detection (LOD) is 0.050 µM. Formation of 1:1 metal-to-ligand complex, [ZnL], has been ascertained by X-ray crystallography, Mass, Job's composition study. The complex, [ZnL]

has shown selective INHIBIT logic gate towards H_2PO_4^- . The practical applicability of H_2L has been examined in the identification of Zn^{2+} and H_2PO_4^- in intracellular fluid in living cells (African Monkey Vero Cells).

Supplementary materials

The synthesis (**Scheme S1**); the spectral data of H_2L (^1H NMR, **Fig. S1**; Mass, **Fig. S2**; FT-IR, **Fig. S3**); the spectral data of ZnL (Mass, **Fig. S4**; FT-IR, **Fig. S5**), comparison of emission of $[\text{H}_2\text{L}]$ and $[\text{ZnL}]$ under illumination in UV chamber (**Fig. S6**); Job's plot (**Fig. S7**), Effect of pH on the fluorescence activity of H_2L and H_2L with Zn^{2+} in MeOH-Water (v/v, 2:1) at 530 nm (**Fig. S8**), Fluorescence spectrum of H_2L (**Fig. S9**), fluorescence intensity comparison plot of different metal ions (**Fig. S10**), Benesi-Hildebrand plot (**Fig. S11**), Limit of optical detection (LOD) (**Fig. S12**), Mass spectra of ZnL with H_2PO_4^- (**Fig. S13**), Proposed Chelation Enhancement of Fluorescence (CHEF) and restricted PET upon coordination of probe to Zn^{2+} (**Scheme S2**); Crystallographic data of $[\text{ZnL}]$ (**Table S1**), calculated bond parameters of H_2L (**Table S2**) and $[\text{ZnL}]$ (**Table S3**), composition of frontier molecular orbitals of H_2L (**Table S4**) and $[\text{ZnL}]$ (**Tables S5, S6, S7**), Life time data of H_2L and ZnL complex (**Table S8**). Crystallographic data for the structure has been deposited with the Cambridge Crystallographic Data center, **CCDC No.1425924**. Copies of this information may be obtained free of charge from the Director, CCDC, 12 Union Road, Cambridge CB2 1EZ, UK (e-mail: deposit@ccdc.cam.ac.uk or [www:http://www.ccdc.cam.ac.uk](http://www.ccdc.cam.ac.uk)).

Acknowledgments

Financial support from the West Bengal Department of Science & Technology, Kolkata, India (Sanction No. 228/1(10)/(Sanc.)/ST/P/S&T/9G-16/2012) and the Council of Scientific and Industrial Research (CSIR, Sanction No. 01(2731)/13/EMR-II), New Delhi, India are

gratefully acknowledged. One of us (C. Patra) thanks University Grants Commission, New Delhi for fellowship.

References

- 1 I. Bertini, H. B. Gray, S. J. Lippard, J. S. Valentin, *Bioinorganic Chemistry*, University Science Books, Mill Valley, USA, 1994
- 2 (a) J. M. Berg and Y. Shi, *Science*, 1996, **271**, 1081; (b) X. Xie and T. G. Smart, *Nature*, 1991, **349**, 521 - 524; (c) C. J. Frederickson, J.-Y. Koh and A. I. Bush, *Nat. Rev. Neurosci.*, 2005, **6**, 449 - 462.
- 3 W. J. Bettger and B. L. O' Dell, *J. Nutr. Biochem.*, 1993, **4**, 194 - 207.
- 4 A. I. Bush, *Curr. Opin. Chem. Biol.*, 2000, **4**, 184 - 191
- 5 (a) P. J. Fraker and L. E. King, *Annu. Rev. Nutr.*, 2004, **24**, 277 - 298; (b) C. F. Walker and R. E. Black, *Annu. Rev. Neurosci.*, 2004, **24**, 255 - 275; (c) D. W. Choi and J. Y. Koh, *Annu. Rev. Neurosci.*, 1998, **21**, 347 - 375; (d) J. H. Weiss, S. L. Sensi and J. Y. Koh, *Trends Pharmacol. Sci.*, 2000, **21**, 395 - 401.
- 6 S. L. Galasso and R. H. Dyck, *Mol. Med.*, 2007, **13**, 380 - 387.
- 7 (a) L. C. Costello, Y. Liu, J. Zou and R. B. Franklin, *J. Biol. Chem.*, 1999, **274**, 17499 - 17504; (b) S. M. Henshall, D. E. H. Afar, K. K. Rasiah, L. G. Horvath, K. Gish, I. Caras, V. Ramakrishnan, M. Wong, U. Jeffry and J. G. Kench, *Oncogene*, 2003, **22**, 6005 - 6012.
- 8 (a) A. Ceresa, A. Radu, S. Peper, E. Bakker and E. Pretsch, *Anal. Chem.*, 2002, **74**, 4027 - 4036; (e) R. Martinez-Manez and F. Sancenon, *Chem. Rev.*, 2003, **103**, 4419 - 4476.
- 9 (a) L. Tang, M. Cai, P. Zhou, J. Zhao, K. Zhong, S. Hou and Y. Bian *RSC Adv.*, 2013, **3**, 16802-16809 ;; (b) Z. Dong, X. Le, P. Zhou, C. Dong and J. Ma, *RSC Adv.*, 2014, **4**,

- 18270–18277.; (c) G. J. Park, Y. J. Na, H. Y. Jo, S. A. Lee, A. R. Kim, I. Nohb and C. Kim, *New J. Chem.*, 2014, 38, 2587--2594.; (d) G. R. C. Hamilton, Y. Sheng, B. Callan, R. F. Donnelly and J. F. Callan, *New J. Chem.*, 2015, 39, 3461--3466
- 10 (a) M. Kumar, R. Kumar and V. Bhalla, *Chem. Commun.*, 2009, 7384-7386; (b) M. Kumar, N. Kumar, V. Bhalla, P. R. Sharma and Y. Qurishi, *Chem. Commun.*, 2012, **48**, 4719 - 4721.
- 11 A K Bhanja, C Patra, S Mondal, D Ojha, D Chattopadhyay and C Sinha, *RSC Adv.*, 2015, **5**, 48997 – 49005.
- 12 S Mondal, A K Bhanja, D Ojha, T K Mondal, D Chattopadhyay and C Sinha, *RSC Adv.*, 2015, **5**, 73626 – 73638.
- 13 A. K. Gupta, A. Dhir, and C. P. Pradeep, *Eur. J. Org. Chem.* 2015, 122–129
- 14 (a) C. P. Mathews and K. E. van Hold, *Biochemistry*, The Benjamin/Cummings Publishing Company, Inc., Redwood City, CA, 1990; (b) J. M. Paredes, M. D. Giron, M. J. Ruedas-Rama, A. Orte, L. Crovetto, E. M. Talavera, R. Salto, and J. M. Alvarez-Pez, *J. Phys. Chem. B.*, 2013, **117**, 8143–8149.
- 15 S. E. Manhan, *Fundamentals of Environmental Chemistry*, Third Edition, CRC Press, Taylor & Francis Group, LLC, 2008.
- 16 M. P. Okoh, J. L. Hunter, J. T. Corrie, and M. R. Webb, *Biochemistry*, 2006, **45**, 14764-14771.
- 17 S. E. Manhan, *Fundamentals of Environmental Chemistry*, Third Edition, CRC Press, Taylor & Francis Group, LLC, 2008.
- 18 S. H. Hong, S. J. Park, S. Lee, S. Kim, M. H. Cho, *J. Toxicol. Sci.* 2015, **40**, 55-69.
- 19 (a) J. Yoon, S. K. Kim, N. J. Singh, J. W. Lee, Y. J. Yang, K. Chellappan, and K. S. Kim, *J. Org. Chem.*, 2004, **69**, 581-583; (b) K. Ghosh, D. Kar, S. Joardar, D. Sahu and B.

- Ganguly, *RSC Adv.*, 2013, **3**, 16144–16151; (c) N. Sharma, S. I. Reja, V. Bhalla and M. Kumar, *Dalton Trans.*, 2015, **44**, 6062–6068; (d) D. Zhang, J. R. Cochrane, A. Martinez and G. Gao, *RSC Adv.*, 2014, **4**, 29735–29749; (e) S. Xu, M. He, H. Yu, X. Cai, X. Tan, B. Lu and B. Shu, *Anal. Biochem.*, 2001, **299**, 188–193; (f) G. Ambrosi, M. Formica, V. Fusi, L. Giorgi, A. Guerri, E. Macedi, M. Micheloni, P. Paoli, R. Pontellini, and P. Rossi, *Inorg. Chem.*, 2009, **48**, 5901–5912; (g) K. Xu, Z. Chen, L. Zhou, O. Zheng, X. Wu, L. Guo, B. Qiu, Z. Lin, and G. Chen, *Anal. Chem.*, 2015, **87**, 816–820; (h) I. Ravikumar, P. Ghosh, *Inorg. Chem.*, 2011, **50**, 4229–4231; (i) C. Solscheid, S. Kunzelmann, C. T. Davis, J. L. Hunter, A. Nofer, and M. R. Webb, *Biochemistry*, 2015, **54**, 5054–5062; (j) S. Khatua, S. H. Choi, J. Lee, K. Kim, Y. Do, and D. G. Churchill, *Inorg. Chem.* 2009, **48**, 2993–2999; (k) J. M. Paredes, M. D. Giron. M. J. Ruedas-Rama, A. Orte, L. Crovetto, E. M. Talavera, R. Salto, and J. M. Alvarez-Pez, *J. Phys. Chem. B.*, 2013, **117**, 8143–8149; (l) G. Saikia and P. K. Iyer, *Macromolecules*, 2011, **44**, 3753–3758; (m) H. N. Lee, K. M. K. Swamy, S. K. Kim, J. –Y. Kwon, Y. Kim, S. –J. Kim, Y. J. Yoon, and J. Yo, *Org. Let.*, 2007, **9**, 243–246.
- 20 C Patra, A K Bhanja, C Sen, D Ojha, D Chattopadhyay, A Mahapatra, and C Sinha, *Sensors and Actuators B*, 2016, **228**, 287–294
- 21 G. M. Sheldrick, *Acta Cryst A.*, 2008, **64**, 112–122.
- 22 J. Farrugia, *J. Appl. Cryst.* 1997, **30**, 565 - 565.
- 23 A. L. Spek, *PLATON*, The Netherlands, 1999.
- 24 M. J. Frisch, G. W. Trucks, H. B. Schlegel, G. E. Scuseria, M. A. Robb, J. R. Cheeseman, G. Scalmani, V. Barone, B. Mennucci, G. A. Petersson, H. Nakatsuji, M. Caricato, X. Li, H. P. Hratchian, A. F. Izmaylov, J. Bloino, G. Zheng, J. L. Sonnenberg, M. Hada, M.

Ehara, K. Toyota, R. Fukuda, J. Hasegawa, M. Ishida, T. Nakajima, Y. Honda, O. Kitao, H. Nakai, T. Vreven, J. A. Montgomery Jr., J. E. Peralta, F. Ogliaro, M. Bearpark, J. J. Heyd, E. Brothers, K. N. Kudin, V. N. Staroverov, R. Kobayashi, J. Normand, K. Raghavachari, A. Rendell, J. C. Burant, S. S. Iyengar, J. Tomasi, M. Cossi, N. Rega, J. M. Millam, M. Klene, J. E. Knox, J. B. Cross, V. Bakken, C. Adamo, J. Jaramillo, R. Gomperts, R. E. Stratmann, O. Yazyev, A. J. Austin, R. Cammi, C. Pomelli, J. W. Ochterski, R. L. Martin, K. Morokuma, V. G. Zakrzewski, G. A. Voth, P. Salvador, J. J. Dannenberg, S. Dapprich, A. D. Daniels, O. Farkas, J. B. Foresman, J. V. Ortiz, J. Cioslowski, D. J. Fox, GAUSSIAN 09, Revision D.01, Gaussian Inc., Wallingford, CT, 2009.

- 25 A.D. Becke, *J. Chem. Phys.*, 1993, **98**, 5648-5652.
- 26 C. Lee, W. Yang, R.G. Parr, *Phys. Rev. B.*, 1988, **37**, 785 - 789.
- 27 P. J. Hay, W. R. Wadt, *J. Chem. Phys.*, 1985, **82**, 270 - 283.
- 28 W. R. Wadt, P. J. Hay, *J. Chem. Phys.*, 1985, **82**, 284-298.
- 29 P. J. Hay, W. R. Wadt, *J. Chem. Phys.*, 1985, **82**, 299 - 310.
- 30 V. Barone, M. Cossi, *J. Phys. Chem. A*, 1998, **102**, 1995 – 2001.
- 31 M. Cossi, V. Barone, *J. Chem. Phys.*, 2001, **115**, 4708 – 4717.
- 32 M. Cossi, N. Rega, G. Scalmani, V. Barone, *Energies, J. Comput. Chem.*, 2003, **24**, 669 - 681.
- 33 N.M. O'Boyle, A.L. Tenderholt, K.M. Langner, *J. Comput. Chem.*, 2008, **29**, 839 - 845.
- 34 P. Mondal, R. Sarkar, A. Hens and K. K. Rajak, *RSC Adv.*, 2014, **4**, 38769 - 38782.

- 35 P. Bag, D. Chattopadhyay, H. Mukherjee, D. Ojha, N. Mandal, M. Sarkar Chawla, T. Chatterjee, G. Das and S. Chakraborti, *Virology J.*, 2012, **9**, 98-109.
- 36 G. Rajsekhar, C. Rao, P. Saarenketo, K. Nattinen and K. Rissanen, *New. J. Chem.*, 2004, **28**, 75–84.
- 37 S. Saha (Halder), C. Sen, S. Roy, D. Mallick. E. López-Torres, C. Sinha, *Polyhedron*, 2015, **97**, 240–247.
- 38 (a) A. Hens and K. K. Rajak, *RSC Adv.*, 2015, **5**, 4219–4232; (b) H. Mandal, S. Chakraborty and D. Ray, *RSC Adv.*, 2014, **4**, 65044–65055; (c) H. S. Jena, *RSC Adv.*, 2014, **4**, 3028–3044.
- 39 X. Shang, H. Wu, S. Jia, J. Han, Y. Liu, Z. Yin, X. Qin, J. Zhang and X. Xu, *J. Chil. Chem. Soc.*, 2013, **58**, 3.
- 40 J. Jiang, H. Jiang, X. Tang, L. Yang, W. Dou, W. Liu, R. Fang and W. Liu, *Dalton Trans.* 2011, **40**, 6367–6370.
- 41 P. Li, X. Zhou, R. Huang, L. Yang, X. Tang, W. Dou, Q. Zhao and W. Liu, *Dalton Trans.*, 2014, **43**, 706–713.
- 42 S. Xiao, Z. Liu, J. Zhao, M. Pei, G. Zhang and W. He, *RSC Adv.*, 2016, **6**, 27119-27125
- 43 T. Mukherjee, J. C. Pessoa, A. Kumar and A. R. Sarkar, *Dalton Trans.* 2012, **41**, 5260–5271.
- 44 A. Ajayaghosh, P. Carol and S. Sreejith, *J. Am. Chem. Soc.*, 2005, **127**, 14962–14963.

- 45 Y. Liu, Q. Fei, H. Shan, M. Cui, Q. Liu, G. Feng and Y. Huan , *Analyst*, 2014, **139**, 1868–1875.
- 46 J.Guan, P. Zhang, T. Wei, Q. Lin, H. Yao and Y. –M. Zhang, *RSC Adv.*, 2014, **4**, 35797–35802.
- 47 S. A. Ingale, F. Seela, *J. Org. Chem.*, 2012, **77**, 9352-9356.
- 48 V. Bhalla, R. Tejpal and M. Kumar, *Dalton Trans.*, 2012, **41**, 10182–10188.
- 49 S. S. Mati, S. Chall, S. Konar, S. Rakshit, S. C. Bhattacharya, *Sens. Actuators, B*. 2014, **201**, 204-212.
- 50 Z. Zhang, F. –W. Wang, S. –Q. Wang, F. Ge, B.-X. Zhao and J. –Y. Miao , *Org. Biomol. Chem.*, 2012, **10**, 8640–8644.
- 51 A. Ciupa, M. F. Mahon, P. A. De Bank and L. Caggiano , *Org. Biomol. Chem.*, 2012, **10**, 8753–8757.
- 52 S. –Y. Jiao, L. –L. Peng, K. Li, Y.-M. Xie, M. –Z. Ao, X. Wang and X. –Q. Yu, *Analys.t*, 2013, **138**, 5762–5768.
- 53 Z. Xu, J. Yoon and D. R. Spring , *Chem. Soc. Rev.*, 2010, **39**, 1996–2006.
- 54 G. Sivaraman, T. Anand and D. Chellappa , *Analyst*. 2012, **137**, 5881–5884.
- 55 A. Ghorai , J. Mondal , R. Chandra , G. K. Patra , *Dalton Trans* , 2015, **44** , 13261-13271.

- 56 S. Suganya, S. Velmathi, P. Venkatesan, S.P. Wub and M. S. Boobalanc, *Inorg. Chem. Front.*, 2015, **2**, 649-656.
57. A. P. de Silva, Molecular Logic Gates in “Supramolecular Chemistry: From Molecules to Nanomaterials” J. W. Steed and P. A. Gale (Eds), John Wiley & Sons Ltd., 2012.
58. D. Sarkar, A. Pramanik, S. Biswas, P. Karmakar and T. K. Mondal *RSC Adv.*, 2014, **4**, 30666–30672.

Table of Content

Imine functionalized thioether Zn(II) turn-on fluorescent sensor and selective sequential logic operations with H_2PO_4^- ; DFT computation and live cell imaging

Chiranjit Patra, Anup Kumar Bhanja, Chandana Sen, Durbadal Ojha, Debprasad Chattopadhyay, Ambikesh Mahapatra, and Chittaranjan Sinha*

Thioether Schiff base (H_2L), a nontoxic Zn^{2+} sensor (LOD, $0.050 \mu\text{M}$) has shown selective ON – OFF emission following INHIBIT logic circuit with H_2PO_4^- and useful agent for the identification of Zn^{2+} and H_2PO_4^- in intracellular fluid in living cells.

